Design, Synthesis, and Multiple Hierarchical Ordering of a Novel Side-Chain Liquid Crystalline-Rod Diblock Copolymer

ARTICLE *in* MACROMOLECULES · NOVEMBER 2009

Impact Factor: 5.8 · DOI: 10.1021/ma9017668

6 AUTHORS, INCLUDING:

He-Lou Xie
Xiangtan University
12 PUBLICATIONS **101** CITATIONS
SEE PROFILE

Yi-Xin Liu
Fudan University
11 PUBLICATIONS **180** CITATIONS
SEE PROFILE

8774 *Macromolecules* **2009**, *42*, 8774–8780
DOI: 10.1021/ma9017668

Macromolecules
ARTICLE

Design, Synthesis, and Multiple Hierarchical Ordering of a Novel Side-Chain Liquid Crystalline-Rod Diblock Copolymer

He-Lou Xie,[†,‡] Yi-Xin Liu,[‡] Guan-Qun Zhong,[†] Hai-Liang Zhang,*[,†] Er-Qiang Chen,*[,‡] and Qi-Feng Zhou[‡]

[†]*Key Laboratory of Polymeric Materials and Application Technology of Hunan Province, Key Laboratory of Advanced Functional Polymer Materials of Colleges, and Universities of Hunan Province, College of Chemistry, Xiangtan University, Xiangtan 411105, Hunan Province, China, and* [‡]*Beijing National Laboratory for Molecular Sciences, Department of Polymer Science and Engineering, and Key Laboratory of Polymer Chemistry and Physics of Ministry of Education, College of Chemistry and Molecular Engineering, Peking University, Beijing 100871, China*

Received August 7, 2009; Revised Manuscript Received October 15, 2009

ABSTRACT: A novel double liquid crystalline (LC) block copolymer (BCP) composed of poly[ω-(4′-methoxybiphenyl-4-yloxy)hexyl methacrylate] (PMBHMA) and poly{2,5-bis[(4-meth-oxyphenyl)oxy-carbonyl]styrene} (PMPCS) was designed and successfully synthesized by reversible addition−fragmentation chain transfer (RAFT) polymerization. Whereas PMBHMA is a conventional side-chain LC (SCLC) polymer, PMPCS is a typical mesogen-jacketed LC polymer, which can serve as rod after it forms columnar LC (Φ) phase. Therefore, the PMBHMA-*b*-PMPCS is an SCLC−rod BCP. The phase structures and transitions of the PMBHMA-*b*-PMPCS synthesized with a PMPCS volume fraction of ∼49% were investigated using various techniques including thermal analysis and X-ray scattering and diffraction methods. A microphase-separated lamellar morphology was identified for this SCLC−rod sample. The Φ phase of the PMPCS block with the rod direction perpendicular to the interface remained unchanged and impacted the LC transitions of PMBHMA blocks greatly. We found that the smectic A phase of the PMBHMA disappeared, and meanwhile, its nematic phase got stabilized over a wide temperature range. At low temperatures, small smectic E domains with homogeneous orientation formed in the PMBHMA block domains. Our work demonstrates that the confinement imposed by the rod block and dimension commensurability of the ordered structures are indeed crucial for SCLC−rod BCPs.

Introduction

The design and synthesis of block copolymers (BCPs) containing liquid crystalline (LC) polymer with electro-optical properties, such as rod−coil and side-chain LC (SCLC)−coil, has been paid great attention in the past two decades.[1−5] These BCPs naturally present hierarchical orderings on two different length scales, that is, the microphase separation with domain size ranged from a few to tens of nanometers and the LC packing confined in the phase domains. On the basis of thoroughly experimental and theoretical studies of amorphous coil−coil BCPs, it is well understood that the interplay of the minimization of the interfacial energy and the maximization of the coil entropy determines the microphase-separated structures.[6,7] Once the LC segments are introduced, additional interactions associated with LC packing may affect the phase behavior of the BCPs. For example, it has been reported that some SCLC−coil diblocks may possess the order−disorder transition temperature (T_{ODT}) identical to the LC-isotropic temperature ($T_{LC\text{-}i}$) of the SCLC block.[8−14] Compared with their amorphous coil−coil counterparts, the composition region and stability of the lamellar phase may be enhanced in some LC BCPs, particularly in the rod−coil ones.[15−18] The confinement effect can also greatly impact the LC behavior; for example, when confined in spherical microdomains, the SCLC blocks may just form the less-ordered nematic (N) phase rather than the smectic A (SmA), which is stable in the continuous phase.[19] It is expected that combination of microphase separation and liquid crystallinity can lead to new materials with superior properties amenable to practical application.[1] For example, it is realized that the LC segments usually exhibit a preferential orientation (either homogeneous or homeotropic) with respect to the interface.[1,11,20−28] Therefore, proper orientation of the microdomains can result in desired alignment of the LC segments, which facilitates the LC BCPs as great candidates for advanced technologies.

From a chemical point of view, many other types of LC BCPs beyond rod−coil and SCLC−coil, such as SCLC−SCLC, SCLC−rod, and rod−rod, can be achieved.[1] Particularly owing to the great advance of "living" radical polymerization, LC BCPs with controlled molecular weight (MW) and composition can be successfully synthesized using vinyl monomers. For example, upon using the reversible addition−fragmentation chain transfer (RAFT) polymerization method, Y. Zhao et al. have recently synthesized a SCLC−SCLC BCP with the two blocks bearing two different mesogenic groups of azobenzene and biphenyl, respectively.[29] It is interesting to note that for this double SCLC BCP, the photoinduced orientation of azobenzene mesogens can propagate into the biphenyl-containing domains through the interface, and thus the two mesogens finally share the same orientation. In this work, we intend to propose a facile synthetic strategy of BCP containing a SCLC block and a rod block, namely, SCLC−rod BCP, on the basis of "living" radical polymerization.

Although several SCLC−rod BCPs have been reported in the literature,[30−32] the synthesis with precise control of the chemical

*To whom the correspondence should be addressed. E-mail: zhanghailiang@xtu.edu.cn (H.-L.Z.); eqchen@pku.edu.cn (E.-Q.C.).

 Published on Web 10/29/2009

structure and composition still remains a challenge; therefore, the understanding of the phase behavior of such double LC BCPs on different length scales is rather limited so far. The sample reported herein is composed of two blocks of poly[ω-(4′-methoxybiphenyl-4-yloxy)hexyl methacrylate] (PMBHMA) and poly{2,5-bis-[(4-methoxyphenyl)oxycarbonyl]styrene} (PMPCS). As a conventional SCLCP, the LC properties of PMBHMA are largely determined by the side chains with biphenyl moieties.[33,34] It is worth mentioning that the block of PMPCS, which acts as the rod in the BCP, is a typical mesogen-jacketed LC polymer (MJLCP).[35−37] At the molecular structure level of MJLCP, the bulky mesogenic groups are laterally attached to the flexible backbone via a single carbon−carbon bond. Consequently, the strong steric hindrance imposed by the side chains forces the main chain to be well extended, leading to the rod-like chain, which can pack into columnar LC (Φ) phases.[38,39] Recently, we have demonstrated that several BCPs containing PMPCS are rod−coil, which form hierarchical ordering structure with microphase separation and Φ phase of the PMPCS within the microdomains.[40−42]

For the PMBHMA-*b*-PMPCS sample studied, microphase-separated lamellar structure and homeotropic orientation of PMPCS rods packing in the Φ phase were evidenced by our X-ray experiments, which remained unchanged despite the LC transitions of the PMBHMA block. Because the cross-sectional area per block was determined by the PMPCS rod, the PMBHMA blocks experienced a significant lateral constrain in addition to the confinement imposed along the lamellar normal. The SmA phase, which exists in homo-PMBHMA[33,34] and a coil−SCLC BCP composed of polystyrene (PS) and PMBHMA (PS-*b*-PMBHMA),[33] was not observed in the diblock. This phenomenon could be ascribed to the mismatch between the rod diameter and the smectic layer spacing. The N phase of the PMBHMA became stable over a wide temperature range. When the interaction between biphenyl groups enhanced with lowering temperature, small smectic E (SmE) domains of the PMBHMA block with homogeneous orientation could form. Our work demonstrates that the confinement imposed by the rod block and dimension commensurability of the ordered structure is indeed crucial for the SCLC−rod BCP.

Experimental Section

Synthesis. *Materials.* 1,6-Dibromohexane (98%, Alfa Aesar), 4,4-biphenol (98%, Alfa Aesar), *N*,*N*-dimethylformamide (DMF) (Shanghai Chemical Reagents Co., A.R. grade), dimethyl sulfate (98%, Alfa Aesar), carbon disulfide (Aldrich, 99% anhydrous), phenylmagnesium bromide (1 N in THF, Aldrich), and 2,2′-azobis (2-methylpropionitrile) (AIBN, 99%, Aldrich) were used as received. Chlorobenzene (Acros, 99%) was purified by washing with concentrated sulfuric acid to remove residual thiophenes, followed by washing twice with water, once with 5% sodium carbonate solution, and again with water before being dried with anhydrous calcium chloride and then distilled. Acetone (AR, Beijing Chemical) was refluxed over potassium permanganate and distilled before use.

Synthesis of Chain Transfer Agent (CTA) 2-(2-Cyanopropyl)dithiobenzoate (CPDB). CPDB was synthesized using the procedure described by Winnik et al.[43] ^{1}H NMR (400 MHz, δ, $CDCl_3$): 7.85−7.93 (d, 2H, C_6H_4), 7.50−7.60 (m, 1H, C_6H_4), 7.30−7.40 (m, 2H, C_6H_4), 1.90−1.93 (s, 6H, $-CH_3$).

Synthesis of Monomers MBHMA and MPCS. MBHMA was prepared using the procedure described by Okamoto et al.[44] ^{1}H NMR (400 MHz, δ, $CDCl_3$): 7.51 (m, aromatic, 4H), 66.9, (m, aromatic, 4H), 4.2, 4.0 (t, OCH_2, H), 3.8 (s, OCH_3, 3H), 2.0 (s, CCH_3, 3H), 1.8−1.7 (q, OCH_2CH_2, 4H), 1.4−1.6 (m, $PhOCH_2CH_2CH_2CH_2$, 4H). MPCS was prepared using the procedure described by Zhang et al.[45] ^{1}H NMR, (400 MHz, δ, $CDCl_3$): 8.18−8.44 (m, 3H of phenyl), 7.51−7.54 (q, 1H of $-CH=$), 6.95−7.18 (m, 8H of phenyl), 5.47−5.86 (2 d, 2H of dCH_2), 3.83 and 3.84 (2 s, 6H of $-OCH_3$).

Scheme 1. Synthetic Route and Schematic Representation of SCLC−rod Diblock Copolymer of PMBHMA-*b*-PMPCS

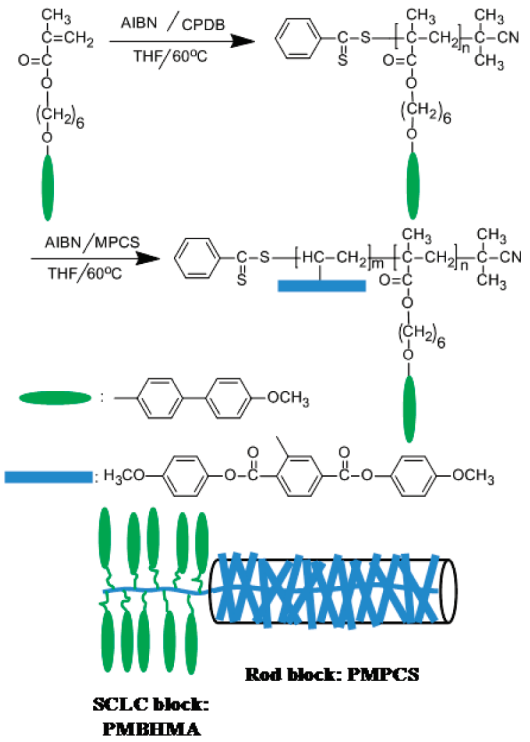

Synthesis of Diblock Copolymer. The synthetic route of the PMBHMA-*b*-PMPCS is described in Scheme 1. To prepare the first block, MBHMA (1.16 g, 3 mmol), AIBN (3.3 mg, 0.02 mmol), and CPDB (13 mg, 0.06 mmol) were added to a reaction tube, followed by the addition of 3 mL of THF. After being degassed with three freeze−thaw cycles, the tube was sealed under vacuum. The polymerization was carried out at 60 °C for 4 h. Afterward, the reaction solution was diluted with dichloromethane and was then dripped into methanol. The polymer precipitate was further purified by repeated dissolution in dichloromethane and precipitation in methanol three times. The obtained PMBHMA was dried in a vacuum oven at room temperature for 24 h before use. The gel permeation chromatography (GPC) measurement indicated that the PMBHMA possessed a low polydispersity index (PDI) of 1.19 and an apparent number-average MW (M_n) of 2.68×10^4 g/mol.

The target diblock copolymer was synthesized through the RAFT chain extension reaction using the PMBHMA with a chain end of dithiobenzoate as the macromolecular CTA (PMBHMA-CTA). In typical, MPCS (60.6 mg, 0.15 mmol), AIBN (0.4 mg, 0.0025 mmol), and PMBHMA-CTA (3.75 mg, 0.0075 mmol) were added to 3 mL of THF. The polymerization condition and the purification procedure were the same as that used for the synthesis of PMBHMA block. The apparent M_n and PDI of the resultant diblock were measured to be 5.08×10^4 g/mol and 1.26, respectively.

Instruments and Measurements. GPC measurements were carried out at 35 °C on a Waters 1515 instrument equipped with three Waters μ-Styragel columns (10^3, 10^4, and 10^5 Å) in series, using THF as the eluent at a flow rate of 1.0 mL/min. The GPC data were calibrated with PS standards. ^{1}H NMR spectra were recorded on a Bruker ARX 400 MHz spectrometer with tetramethylsilane (TMS) as the internal standard and $CDCl_3$ as the solvent. The density measurements of the home-PMBHMA (PMBHMA-CTA) sample were conducted using a floatation technique. A mixture of tetrachloride and petroleum ether at room temperature was used. After the buoyancies of the sample

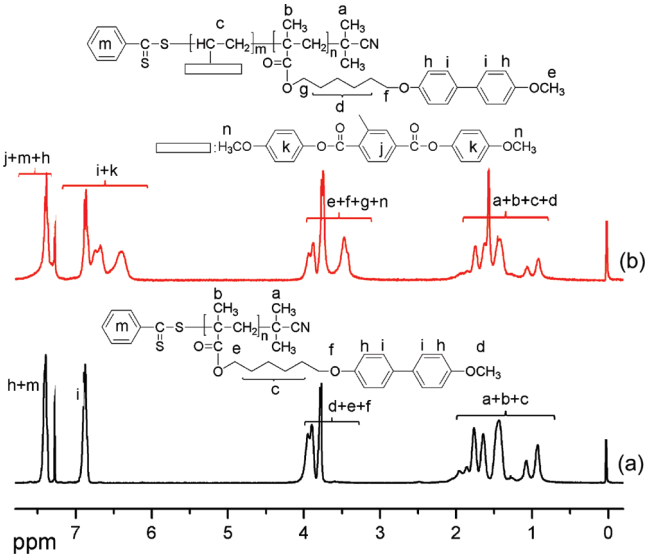

Figure 1. ^{1}H NMR spectra of (a) PMBHMA-CTA and (b) PMBHMA-*b*-PMPCS. The assignments of the resonance peaks are indexed.

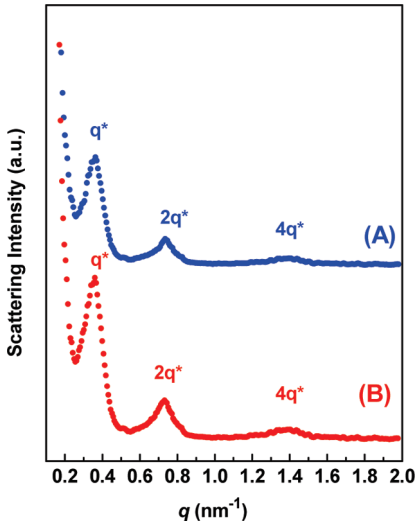

Figure 2. SAXS profiles of PMBHMA-*b*-PMPCS recorded after the sample annealed at 185 °C for 2 h: (A) at 185 °C and (B) at room temperature.

and the surrounding solvent mixture were matched, the sample was floated freely for an extended period of time. A pycnometer was then filled with the solution mixture to be weighed.

Differential scanning calorimetry (DSC, PerkinElmer Pyris I) was employed to study the phase transitions of the samples. The temperature and heat flow were calibrated with benzoic acid and indium. The samples were encapsulated in hermetically sealed aluminum pans with a typical sample weight of ~2 mg. The cooling and subsequent heating DSC experiments were carried out at a rate of 10 °C/min.

To identify the microphase-separated structure, we performed 1D small-angel X-ray scattering (SAXS) experiment with a high-flux SAXS instrument (SAXSess, Anton Paar) equipped with Kratky block-collimation system and a Philips PW3830 sealed-tube X-ray generator (Cu Kα). The scattering pattern was recorded on an imaging plate (IP) with a pixel size of 42.3 × 42.3 μm^2, of which the peak positions were calibrated with silver behenate. After background subtraction, desmearing was performed according to the Lake's method. A temperature control unit (Anton Paar TCS300) in conjunction with the SAXSess was utilized to study the structure at various temperatures.

The LC phase behaviors of both the PMHBMA and PMPCS blocks were examined by wide-angle X-ray diffraction (WAXD) thermal experiments. 1D powder patterns were obtained by using a Philips X'Pert Pro diffractometer with an X'celerator detector in a reflection mode. To identify the LC phase orientation, we prepared the oriented samples by mechanical shearing at 200 °C, and the 2D WAXD experiments were performed with a Bruker D8Discover in a transmission mode using a GADDS detector. The point-focused X-ray beam was aligned perpendicular to both the shear direction and the shear gradient. For both diffractometers, the X-ray sources (Cu Kα) were provided by 3 kW ceramic tubes, and the diffraction peak positions were calibrated with silicon powder ($2\theta > 15°$) and silver behenate ($2\theta < 10°$). The background scattering was recorded and subtracted from the sample patterns. The sample temperature was controlled within ±1 °C.

Results and Discussion

In principle, one can expect that the diblock of PMHBMA-*b*-PMPCS can be synthesized via various controlled ("living") radical polymerization methods. It has been reported that atom-transfer radical polymerization (ATRP) method readily results in the homopolymers of PMHBMA and PMPCS with controlled MW and MW distribution.[34,46] However, our attempts at using ATRP to synthesize the diblock with the first block of either PMHBMA or PMPCS failed; and the reason is unknown at this moment. We found that the RAFT method was a versatile and facile way to prepare the diblock. In particular, the CTA based on dithiobenzoate moiety works effectively for the monomers of both MHBMA and MPCS. Whereas this CTA has been employed to synthesize the SCLC blocks with chemical structure similar to PMHBMA,[29] this is the first time it has been applied to obtain the MJLCP of PMPCS. Our successful polymerization demonstrates that the large mesogenic substitute on one of the vinyl carbons also does not eliminate the polymerizability of the monomers when the radical polymerization follows the mechanism of RAFT.

The GPC trace of the resultant PMHBMA-*b*-PMPCS is unimodal with a fairly narrow MW distribution (PDI of 1.26). Figure 1 describes the ^{1}H NMR spectra of the PMHBMA-CTA and the diblock, wherein the assignments of resonance peaks are included. Clearly, after the RAFT chain extension reaction, the signals attributed to PMPCS block superimpose on the spectrum of PMHBMA. On the basis of the spectrum of the diblock, the weight fraction of the PMPCS block (f_{MPCS}) can be estimated according to

$$f_{MPCS} = \frac{M_{MPCS} \times (7I_{i+k} - 4I_{e+f+g+n})}{M_{MPCS} \times (7I_{i+k} - 4I_{e+f+g+n}) + M_{MBHMA} \times (8I_{e+f+g+n} - 6I_{i+k})}$$

where M_{MPCS} of 404 and M_{MBHMA} of 386 are the MWs of the repeating units and I_{i+k} and $I_{e+f+g+n}$ are the integral intensities of the signals at 6.4 to 7.1 and 3.4 to 4.2 ppm shown in Figure 1. As a result, the f_{MPCS} was calculated to be 51.6%. The density of the PMBHMA-CTA at room temperature was measured to be 1.13 g/cm^3 by a floatation technique. Taking this data to be approximate and the density of 1.28 g/cm^3 reported for the PMPCS in Φ phase,[38] we calculated that the volume fraction of PMPCS was ~49%.

It has been reported that the rod−coil BCPs based on PMPCS can form microphase-separated lamellar structure over a wide range of composition.[40,41,47] Therefore, a lamellar morphology can be expected for this symmetrical diblock of PMBHMA-*b*-PMPCS. Figure 2 shows the SAXS profiles of the sample studied.

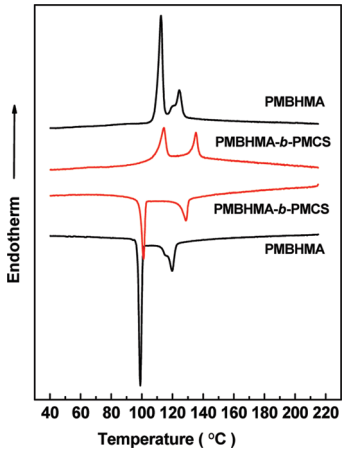

Figure 3. DSC thermograms of the PMBHMA-*b*-PMPCS and PMBHMA-CTA during the first cooling and the second heating at a rate of 10 °C/min. The traces of diblock are plotted after the weight normalization of the PMBHMA block.

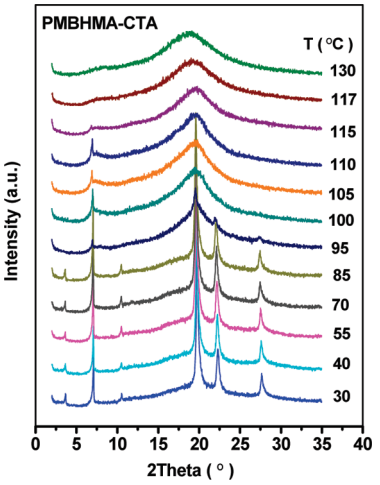

Figure 4. Set of 1D WAXD powder patterns of the PMBHMA-CTA at various temperatures upon cooling.

Before the SAXS experiment, the solution cast sample was subjected to 2 h of annealing at 185 °C, allowing the substantial development of the Φ phase of PMPCS which would then retain permanently regardless of varying temperature. The lamellar morphology is evidenced by the scattering peaks with a q ratio of 1:2:4 ($q = 4\pi \sin\theta/\lambda$, where λ is the X-ray wavelength and 2θ is the scattering angle). The long period corresponding to the first-order scattering is 17.5 nm at 185 °C, where the temperature is sufficiently higher than the $T_{LC\text{-}i}$ of 130 °C of the PMBHMA block. Subsequent cooling to room temperature results in only a trivial shift of the scattering peaks toward higher q position, which may be due to the thermal constriction and the density increase in the PMBHMA domain. This result indicates that LC transitions of the PMBHMA block hardly affect the microphase-separated structure, and moreover, the LC phases can form only within the PMBHMA layer confined by adjacent layers of PMPCS.

Since the Φ phase of the PMPCS block remained unchanged, we focused on the LC transitions of PMBHMA block under the confinement condition. Figure 3 depicts the DSC thermograms of the diblock recorded during cooling and subsequent heating at a rate of 10 °C/min, wherein the DSC traces of PMBHMA-CTA are also included for comparison. The same as those reported in literature for some other homo-PMBHMAs,[34] three enantiotropic transitions can be observed. Upon cooling, the three peak temperatures of exotherms are 119, 115, and 98 °C, respectively. We further performed 1D WAXD thermal experiment of PMBHMA-CTA to verify the LC phase transitions, of which the results are plotted in Figure 4. A typical amorphous pattern is observed at 130 °C. When cooled to 117 °C, the scattering halo in the high-angle region narrows, implying the formation of the N phase. Because the second transition is partially overlapped with the high one of iso-to-N, in addition to further narrowing of the high-angle halo, a tiny peak appears at 2θ of 6.78° (d spacing of 1.30 nm) at 115 °C. This peak increases in intensity with decreasing temperature, which shall be ascribed to the development of the SmA phase. Below 100 °C, the 1D WAXD patterns evidence the SmE structure of PMBHMA. Three peaks with a q ratio of 1:2:3 are at 3.53, 7.03, and 10.36°, respectively, giving the smectic layer period (L_{Sm}) of 2.50 nm. Meanwhile, three strong peaks in the high-angle region can be assigned to be (110), (200), and (210) diffractions of an orthorhombic structure with a = 0.82 nm and b = 0.54 nm.[33] Compared with the calculated fully extended length of 2.2 nm for the side chain, the measured L_{Sm} is only 0.3 nm larger. In this case, to ensure the parallel close packing of the biphenyl groups, the side chains from the two adjacent main-chain sublayers in the smectic structure are largely (but not fully) interdigitated. Note that the first-order layer diffraction is much weaker than the second-order one for the SmE and cannot even be recognized for the SmA. According to Al-Hussein et al.[48] and also Zhu et al.,[49] this diffraction feature indicates that within the smectic structure the electron density at the center portion of the sublayer formed by interdigitated packing of side chains is very close to that of the main-chain sublayer. Combining the DSC and WAXD results, we confirm that the LC transition of PMBHMA-CTA also follows a sequence of SmE ↔ SmA ↔ N ↔ iso.[34]

However, as shown in Figure 3, it is intriguing that the PMBHMA block under the confinement condition renders only two transitions. Moreover, the onsets of transition shift to higher temperatures relative to that of PMBHMA-CTA. This observation implies two opposite effects: one is that the confinement can enhance the stability of the LC phases; the other is that the confinement disfavors the formation of some sort of LC phase. The two LC phases of PMBHMA block were identified using WAXD. Figure 5a collects a set of the 1D WAXD patterns measured upon cooling from 210 to 30 °C. The diffraction peaked at 2θ of 5.84° is characteristic of the PMPCS Φ phase, which can be observed over the entire temperature range examined. Similar to that found in the homo-PMPCS,[38] this diffraction gradually decreases in intensity upon cooling, which may be due to the fact that the periodic electron density contrast generating the Φ phase diffraction reduces with decreasing temperature. Besides the peak at 2θ of 5.84°, the evolution of the diffraction pattern is associated with the LC transitions of the PMBHMA block. Upon cooling to ~130 °C, no additional diffraction peak appears, yet a sudden narrowing and shifting of the halo in the high-angle region is observed. The full width of half-height (fwhh) and the d spacing corresponding to the center position of the halo are plotted in Figure 5b as functions of temperature. The discontinuous changes of the fwhh and d spacing clearly reflect the first-order transition of the PMBHMA block from isotropic to N phase, and the transition temperature is fully consistent with that measured by DSC. With further cooling to < 110 °C, two small diffractions with a q ratio of 1:2 appear at 2θ of 3.51 and 7.03°, respectively. Simultaneously, the (110), (200), and (210) diffractions of the SmE orthorhombic structure emerge from the high-angle halo.[33] Note that no diffraction at ~7.0° corresponding to the SmA of homo-PMBHMA can be detected between 110 and 130 °C. Therefore, we conclude that the within the lamellar microdomain, the SmA phase of PMBHMA is completely suppressed. Consequently, only two LC transitions, that is, SmE ↔ N ↔ iso,

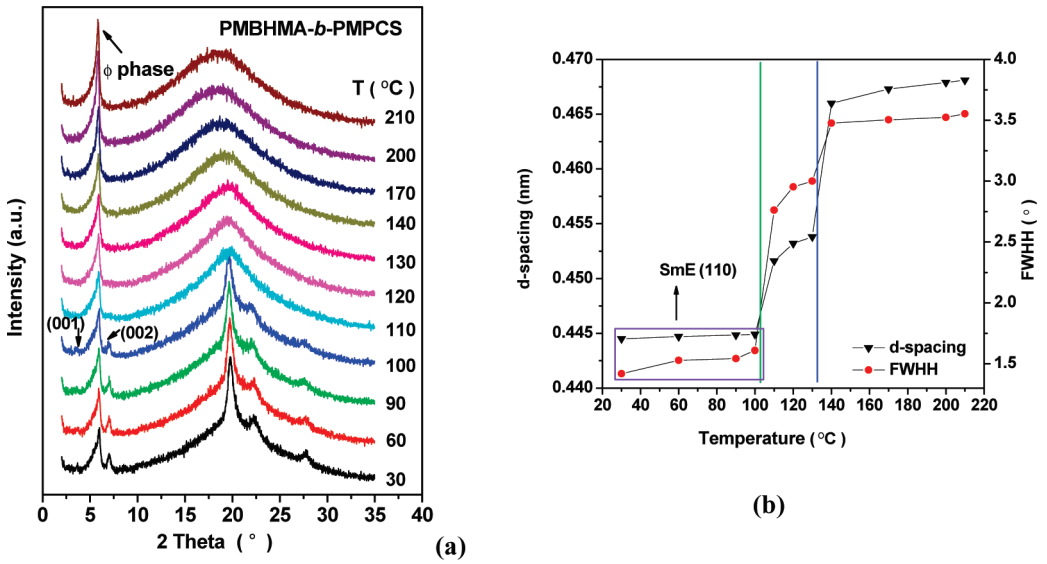

Figure 5. (a) Set of 1D WAXD patterns of PMBHMA-*b*-PMPCS recorded at various temperature during cooling. (b) *d* spacing and full width of half-height (fwhh) of the high angle halo as functions of temperature. Below 110 °C, the data shown in part b correspond to the (110) diffraction of the SmE phase.

can be observed in the diblock, wherein the temperature range of the N phase is much wider than that of PMBHMA-CTA. This phase behavior also makes our SCLC−rod different from PS-*b*-PMBHMA studied by Watanabe et al., of which the SmA phase always exists within the microphase-separated lamellar structure.[33]

It is worth noting that the microphase-separated lamellar morphology of the PMBHMA-*b*-PMPCS permanently remains. Consequently, vanishing of the PMBHMA SmA is not caused by a change of the interface curvature.[19] We presume that interplay of the packing of PMPCS and PMBHMA blocks in the lamellar phase must be crucial. We carried out 2D WAXD experiments to elucidate the geometric correlation of the two blocks. The macroscopic orientation of the diblock was achieved by mechanical shearing at 200 °C. For the other PMPCS-containing BCPs with lamellar morphology, such as PS-*b*-PMPCS[40] and poly(ε-caprolactone)-*b*-PMPCS (PCL-*b*-PMPCS),[41] it is found that mechanical shear is able to result in parallel lamellae with the lamellar normal along the shear gradient. (See the schematic drawing of Figure 6a, wherein *x* and *z* directions are the shear direction and shear gradient, respectively.) Moreover, within the PMPCS domain, the rodlike chains packed in the Φ phase are aligned perpendicular to the lamellar interface.[40,41] Figure 6b−d shows the 2D WAXD patterns of the sheared PMBHMA-*b*-PMPCS sample detected at 180, 120, and 30 °C, respectively, with the X-ray incident beam perpendicular to both the *x* and *z* directions. When the PMBHMA block loses LC ordering, only a pair of sharp diffractions corresponding to a *d* spacing of 1.57 nm is observed on the *x* direction in the low-angle region (Figure 6b), which is attributed to the interference between the rodlike chains with the diffraction direction perpendicular to the column axis of Φ phase. This 2D WAXD result is identical to that reported for the parallel lamellae of PCL-*b*-PMPCS,[41] suggesting that the lamellar normal and the PMPCS rods of the PMBHMA-*b*-PMPCS share the same orientation.

After the PMBHMA block enters its N phase, the low-angle diffraction feature shown in the 2D WAXD pattern (Figure 6c) is largely similar to that of Figure 6b. In the high-angle region, the halo becomes stronger and more concentrated on the *z* direction, which shall be ascribed to the fact that the direction of mesogenic groups of PMBHMA turn to be more parallel to the lamellar interface. Such homogeneous orientation will be further enhanced

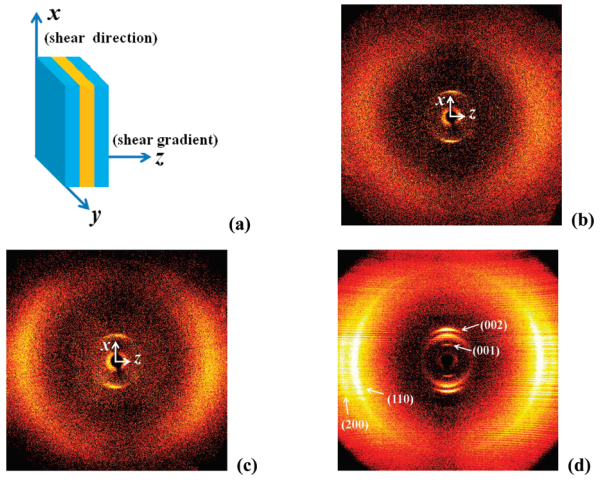

Figure 6. (a) Schematic drawing with *x* and *z* direction, the shear direction, and shear gradient of the parallel lamellae obtained after mechanical shearing. (b,c,d) 2D WAXD patterns of PMBHMA-*b*-PMPCS recorded at 180, 120, and 30 °C, respectively. The X-ray incident beam is directed along the *y* direction.

after the formation of SmE. In Figure 6d of 30 °C, in addition to the diffractions of the PMPCS Φ phase, the first- and second-order diffractions of the SmE layers (indexed as (001) and (002) in Figure 6d) appear on the *x* direction. Meanwhile, the (110) and (200) diffractions from the biphenyl moieties packed in the orthorhombic lattice locating on the *z* direction are observed. This result provides evidence that the SmE layer normal (i.e., direction of the mesogens) and the chain axis of PMPCS rods are orthogonal. On the basis of our WAXD results, Figure 7 depicts the schematic representative of the hierarchical orderings of the PMBHMA-*b*-PMPCS studied.

The 2D WAXD results shown in Figure 6 also indicate that the LC transitions of PMBHMA do not alter the homeotropic orientation of rodlike PMPCS blocks in the microphase-separated lamellar structure. Therefore, the average area per junction (σ_j) is largely determined by the PMPCS rod diameter. The diffraction of 1.57 nm can be assigned as (100) of the Φ phase when the rods pack with a hexagonal symmetry.[41] The calculated diameter of the molecular column or rod is 1.81 nm, and thus the

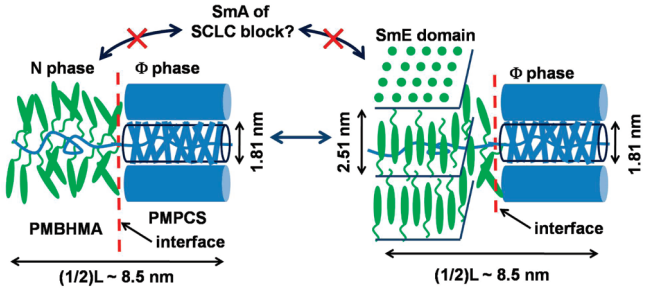

Figure 7. Schematic representation of the hierarchically ordered nanostructures of the PMBHMA-*b*-PMPCS with both blocks packed in their LC phases. Within the microphase-separated lamellar structure, the PMPCS block forms Φ phase; PMBHMA block can form SmE and N phases but not the SmA phase. The biphenyl mesogen and PMPCS rod are oriented parallel and perpendicular to the interface, respectively. The dimensions of the SmE layer period and rod diameter are shown.

average area per junction (σ_j) is ~2.85 nm^2 when a 2D hexagonal lattice at the interface is assumed. In this case, the PMHBMA block packing will be subjected to not only the confinement along the *z* direction but also a lateral constrain due to the limited σ_j, which is nearly constant despite the varying temperature. Considering the orthogonal arrangement of the rod axis and SmE layer normal, as shown in Figure 7, the dimension mismatch between the rod diameter (D_{rod}) of 1.81 nm (or the (100) *d* spacing of 1.57 nm for the Φ phase, which equals to $\sqrt{3}D_{rod}/2$) and the smectic layer period L_{Sm} of 2.51 nm is important. Most likely, this incommensurability disfavors the formation of the SmA phase of the PMHBMA block. On the other hand, the N phase is allowed, of which the stability is even enhanced as a result of the confinement effect.

The existence of SmE shall be associated with the strong interaction between the biphenyl mesogens at low temperature. It has been reported by Al-Hussein et al. that a PS-*b*-PMBHMA with a rather short SCLC block (degree of polymerization (DP) of 6) and a PS weight fraction of 80% can render its microphase-separated lamellar morphology only when the short PMBHMA blocks pack in SmE phase, and after SmE melting, the PS-*b*-PMBHMA enters the disorder phase.[48] This implies that the interaction of the biphenyl groups can even be so strong that a ordered phase morphology gets stabilized. For the PMBHMA-*b*-PMPCS, we consider that the biphenyl interaction substantially increases with lowering temperature, eventually leading to the SmE phase. However, the SmE domains under the confinement condition are much smaller compared with that of the homo-PMBHMA. For the PMBHMA-*b*-PMPCS at room temperature, two apparent correlation lengths, one is along the SmE layer normal and another is along the direction perpendicular to the orthorhombic (110) plane, can be estimated to be ~16 and ~8 nm by using the Scherrer equation. For PMBHMA-CAT, these two correlation lengths are ~44 and ~14 nm, respectively. According to the DSC heating traces shown in Figure 3, we find that the heat of SmE-to-N transition is 10.13 J/g after the weight normalization, which is only 67% of the heat of SmE-to-SmA transition measured for the PMBHMA-CTA. Therefore, the confinement imposed by the PMPCS rods still largely hampers the development of the SmE structure, leading to a low liquid crystallinity of SmE. We presume that the segments of the PMBHMA block near the interface remain in N phase or are even amorphous.

It is worth noting that for the particular PMBHMA-*b*-PMPCS we studied, the ratio of $L_{Sm}/(\sqrt{3}D_{rod}/2)$ is 1.6, implying that the thickness of five smectic layers is equal to that of eight layers of closely packed PMPCS rods. Therefore, it seems that a sort of dimension commensurability can still be realized in our sample. We do not know if it is necessary for the formation of the SmE phase confined between the adjacent layers of PMPCS with the biphenyl groups aligning orthogonal to the rods or if it is just a coincidence. Generally speaking, although the Φ phase of the PMPCS rods dominates the phase behavior in our PMBHMA-*b*-PMPCS, the opposite situation, wherein smectic packing destroys the ordered packing of rods, is also possible. Fully understanding the effect of incommensurability needs more systematical research. The L_{Sm} can be varied by changing the flexible spacer length between the biphenyl mesogen and the polymer backbone, and the D_{rod} can be turned by using the side-on side groups with different chemical structures.[35−38,50,51] Therefore, we shall be able to adjust the ratio of L_{Sm}/D_{rod} (or $L_{Sm}/(\sqrt{3}D_{rod}/2)$) and then examine how large the dimension mismatch will impact the formation of LC phases with rather different geometries. It is also of interest to ask what will be the interplay of the rod and SCLC segments when the BCP exhibits microphase-separated morphologies beyond lamellae. It has been reported that the hierarchical structures of the rod−coil BCPs containing the rod of mesogen-jacketed LC block are greatly affected by varying composition.[51,52] We expect that with a fixed ratio of L_{Sm}/D_{rod} of SCLC−rod BCP, varying the composition may also cause the change of phase morphology, which should be tightly related to the competition of different LC phase formations.

Summary

In summary, we have demonstrated that the controlled radical polymerization of RAFT is a versatile and facile method for the synthesis of LC BCP based on functional vinyl monomers. The new BCP of PMBHMA-*b*-PMPCS reported here belongs to the catalog of SCLC−rod. Whereas the PMBHMA block is a conventional SCLC polymer with the LC properties depending on the side-chain mesogenic groups, the PMPCS block is a typical MJLCP that can serve as a rod when it forms Φ phase. On the basis of our SAXS and WAXD experimental results, we have identified that the symmetrical PMBHMA-*b*-PMPCS sample studied possesses a microphase-separated lamellar morphology, and the Φ phase of PMPCS blocks retains permanently therein with the rod axis perpendicular to the interface. Therefore, the LC transitions of the PMBHMA blocks have to experience two types of confinement: one is imposed by the PMPCS layers, and the other arises from the limited average area per junction largely fixed by the PMPCS rod. As a result, the SmA phase that exists in homo-PMBHMA and PS-*b*-PMBHMA vanishes, which shall be attributed to the mismatch between the rod diameter and the smectic layer spacing. Meanwhile, the temperature window of the N phase is greatly extended. The SmE phase of PMBHMA forms at low temperatures when the biphenyl groups pack in an orthorhombic lattice. However, the SmE domains are rather small, reflecting the fact that the confinements reduce the liquid crystallinity. Currently, the synthesis of PMBHMA-*b*-PMPCS with different MWs and compositions is underway in our laboratory, and a more comprehensive characterization of the phase behavior of the SCLC−rod will be carried out later on. Furthermore, as we discussed above, to elucidate more clearly the effect of dimension mismatch, we shall also design and synthesize the SCLC−rod BCPs with different smectic layer periods and rod diameters.

Acknowledgment. This work was supported by the National Nature Science Foundation of China (NNSFC grants: 20874082, 20774006, and 50573001), the Key Project of Chinese Ministry of Education for Science and Technology (no. 207075), and the Scientific Research Fund of Hunan Provincial Education Department (06A068).

References and Notes

(1) Mao, G.; Ober, C. K. *Acta Polym.* **1997**, *48*, 405–422.

(2) Klok, H. A.; Lecommandoux, S. *Adv. Mater.* **2001**, *13*, 1217–1229.
(3) Ho, R. M.; Chen, C. K.; Chiang, Y. W. *Macromol. Rapid Commun.* **2009**, *30*, 1439–1456.
(4) Cheolmin, P.; Jongseung, Y.; Thomas, E. L. *Polymer* **2003**, *44*, 6725–6760.
(5) Muthukumar, M.; Ober, C. K.; Thomas, E. L. *Science* **1997**, *277*, 1225–1232.
(6) Hamley, I. W. *The Physics of Block Copolymers*; Oxford University Press: Oxford, U.K., 1998.
(7) Bates, F. S.; Fredrickson, G. H. *Phys. Today* **1999**, *52*, 32–38.
(8) Hayakawa, T.; Horiuchi, S. *Angew. Chem., Int. Ed.* **2003**, *42*, 2285–2289.
(9) Ansari, I. A.; Castelletto, V.; Mykhaylyk, T.; Hamley, I. W.; Lu, Z. B.; Itoh, T.; Imrie, C. T. *Macromolecules* **2003**, *36*, 8898–8901.
(10) Anthamatten, M.; Zheng, W. Y.; Hammond, P. T. *Macromolecules* **1999**, *32*, 4838–4848.
(11) Mao, G. P.; Wang, J. G.; Clingman, S. R.; Ober, C. K.; Chen, J. T.; Thomas, E. L. *Macromolecules* **1997**, *30*, 2556–2567.
(12) Tenneti, K. K.; Chen, X. F.; Li, C. Y.; Shen, Z. H.; Wan, X. H.; Fan, X. H.; Zhou, Q. F.; Rong, L. X.; Hsiao, B. S. *Macromolecules* **2009**, *42*, 3510–3517.
(13) Zheng, W. Y.; Hammond, P. T. *Macromolecules* **1998**, *31*, 711–721.
(14) Poser, S.; Fischer, H.; Arnold, M. *Prog. Polym. Sci.* **1998**, *23*, 1337–1379.
(15) Chen, J. T.; Thomas, E. L.; Ober, C. K.; Mao, G.-p. *Science* **1996**, *273*, 343–346.
(16) Olsen, B. D.; Segalman, R. A. *Macromolecules* **2005**, *38*, 10127–10137.
(17) Halperin, A. *Macromolecules* **1990**, *23*, 2724–2731.
(18) Matsen, M. W.; Barrett, C. *J. Chem. Phys.* **1998**, *109*, 4108–4118.
(19) Fischer, H.; Poser, S.; Arnold, M. *Liq. Cryst.* **1995**, *18*, 503–509.
(20) Jenekhe, S. A.; Chen, X. L. *Science* **1999**, *283*, 372–375.
(21) Adams, J.; Gronski, W. *Makromol. Chem.* **1989**, *10*, 553–557.
(22) Tenneti, K. K.; Chen, X. F.; Li, C. Y.; Wan, X. H.; Fan, X. H.; Zhou, Q. F.; Rong, L. X.; Hsiao, B. S. *Macromolecules* **2007**, *40*, 5095–5102.
(23) Olsen, B. D.; Segalman, R. A. *Macromolecules* **2006**, *39*, 7078–7083.
(24) Chen, J. T.; Thomas, E. L.; Ober, C. K.; Hwang, S. S. *Macromolecules* **1995**, *28*, 1688–1697.
(25) Borsali, R.; Lecommandoux, S.; Pecora, R.; Benoit, H. *Macromolecules* **2001**, *34*, 4229–4234.
(26) Zhong, X. F.; Francois, B. *Macromol. Rapid Commun.* **1988**, *9*, 411–416.
(27) Manfred, A.; Sven, P.; Hartmut, F.; Willy, F.; Hermann, U. *Macromol. Rapid Commun.* **1994**, *15*, 487–496.
(28) Lee, M.; Cho, B. K.; Zin, W. C. *Chem. Rev.* **2001**, *101*, 3869–3892.
(29) Zhao, Y.; Qi, B.; Tong, X.; Zhao, Y. *Macromolecules* **2008**, *41*, 3823–3831.
(30) Galli, G.; Chiellini, E.; Laus, M.; Ferri, D.; Wolff, D.; Springer, J. *Macromolecules* **1997**, *30*, 3417–3419.
(31) Guillermain, C.; Gallot, B. *Macromol. Chem. Phys.* **2002**, *203*, 1346–1356.
(32) Galli, G.; Chiellini, E.; Laus, M.; Bignozzi, M. C.; Angeloni, A. S.; Francescangeli, O. *Macromol. Chem. Phys.* **1994**, *195*, 2247–2260.
(33) Yamada, M.; Hirao, A.; Nakahama, S.; Iguchi, T.; Watanabe, J. *Macromolecules* **1995**, *28*, 50–58.
(34) Li, M. H.; Keller, P.; Grelet, E.; Auroy, P. *Macromol. Chem. Phys.* **2002**, *203*, 619–626.
(35) Zhou, Q. F.; Li, H. M.; Feng, X. D. *Macromolecules* **1987**, *20*, 233–234.
(36) Zhou, Q. F.; Li, Z. F.; Zhang, Z. Y.; Pei, X. Y. *Macromolecules* **1989**, *22*, 3821–3823.
(37) Zhou, Q. F.; Zhu, X. L.; Wen, Z. Q. *Macromolecules* **1989**, *22*, 491–493.
(38) Ye, C.; Zhang, H. L.; Huang, Y.; Chen, E. Q.; Lu, Y. L.; Shen, D. Y.; Wan, X. H.; Shen, Z. H.; Cheng, S. Z. D.; Zhou, Q. F. *Macromolecules* **2004**, *37*, 7188–7196.
(39) Wang, X. Z.; Zhang, H. L.; Chen, E. Q.; Wang, X. Y.; Zhou, Q. F. *J. Polym. Sci., Part A: Polym. Chem.* **2005**, *43*, 3232–3244.
(40) Li, C. Y.; Tenneti, K. K.; Zhang, D.; Zhang, H. L.; Wan, X. H.; Chen, E. Q.; Zhou, Q. F.; Carlos, A. O.; Igos, S.; Hsiao, B. S. *Macromolecules* **2004**, *37*, 2854–2860.
(41) Liu, X. B.; Zhao, Y. F.; Chen, E. Q.; Ye, C.; Shen, Z. H.; Fan, X. H.; Cheng, S. Z. D.; Zhou, Q. F. *Macromolecules* **2008**, *41*, 5223–5229.
(42) Gao, L. C.; Yao, J. H.; Shen, Z.; Wu, Y. X.; Chen, X. F.; Fan, X. H.; Zhou, Q. F. *Macromolecules* **2009**, *42*, 1047–1050.
(43) Song, J. S.; Winnik, M. A. *Macromolecules* **2006**, *39*, 8318–8325.
(44) Nakano, T.; Hasegawa, T.; Okamoto, Y. *Macromolecules* **1993**, *26*, 5494–5502.
(45) Zhang, D.; Liu, Y. X.; Wan, X. H.; Zhou, Q. F. *Macromolecules* **1999**, *32*, 5183–5185.
(46) Zhang, H.; Yu, Z.; Wan, X.; Zhou, Q. F.; Woo, E. M. *Polymer* **2002**, *43*, 2357–2361.
(47) Gao, L. C.; Zhang, C. L.; Liu, X.; Chen, X. F.; Wu, Y. X.; Chen, X. F.; Shen, Z. H.; Fan, X. H.; Zhou, Q. F. *Soft Matter* **2008**, *4*, 1230–1236.
(48) Al-Hussein, M.; de Jeu, W. H.; Vranichar, L.; Pispas, S.; Hadjichristidis, N.; Itoh, T.; Watanabe, J. *Macromolecules* **2004**, *37*, 6401–6407.
(49) Zhu, X. Q.; Liu, J. H.; Liu, Y. X.; Chen, E. Q. *Polymer* **2008**, *49*, 3103–3110.
(50) Yin, X. Y.; Ye, C.; Ma, X.; Chen, E. Q.; Qi, X. Y.; Duan, X. F.; Wan, X. H.; Cheng, S. Z. D.; Zhou, Q. F. *J. Am. Chem. Soc.* **2003**, *125*, 6854–6855.
(51) Tenneti, K. K.; Chen, X. F.; Li, C. Y.; Wan, X. H.; Fan, X. H.; Zhou, Q. F.; Rong, L. X.; Hsiao, B. S. *Soft Matter* **2008**, *4*, 458–461.
(52) Tenneti, K. K.; Chen, X. F.; Li, C. Y.; Tu, Y. F.; Wan, X. H.; Zhou, Q. F.; Sics, I.; Hsiao, B. S. *J. Am. Chem. Soc.* **2005**, *127*, 15481–15490.